VISIOPHARM®

Phenoplex: Analysis of a 30-plex assay multiplex image

WHITE PAPER

Case Study: Identifying cytotoxic GZMB+ cells in CD8+ and CD56+ immune lineages in a colorectal cancer sample and analyzing their proximity to epithelial cancer cells.

by Fabian Schneider, James R. Mansfield, Regan Baird

Introduction

Colorectal Cancer (CRC) is one of the most malignant neoplasms, with an increasing tendency in terms of morbidity and deaths in the western world.[1] CRC can be categorized into tumors that are: mismatch repair deficient or have high levels of microsatellite instability (dMMR-MSI high, 15%); and mismatch repair proficient or microsatellite instability low tumors (pMMR-MSI low, 85%). dMMR-MSI high CRC is associated with a high tumor mutational burden and immune cell infiltration.[2,3] Recent studies have shown that immune checkpoint therapy (ICT) targeting PD-1 or CTLA-4 results in improved survival in metastatic dMMR-MSI high CRC, while pMMR-MSI low CRC is largely unresponsive to current ICT. Tumor-infiltrating immune cells, mainly T cells, have been shown to be key components influencing tumor development and metastasis.[4,5]

High densities of activated CD8+ cytotoxic T lymphocytes (CTL) within the tumor niche are associated with favorable prognoses in various cancers, including CRC.[6,7] The main cytotoxic lymphocyte populations are CTL and Natural Killer (NK) cells that destroy harmful cells and mediate antitumor responses. NK cells are part of the innate immune system and can recognize and kill stressed or infected cells without prior sensitization, while CTLs are a part of the adaptive immune system. T cells need priming by antigen-presenting cells, such as B cells, dendritic cells or macrophages, to target and destroy cells presenting specific antigens via MHC class I molecules.[8] T cells recognize and respond to antigens through the interaction between their T cell receptors (TCRs) and the peptide-MHC complex, with CD4 or CD8 co-receptors enhancing this interaction. MHC class I molecules present endogenous peptides to CD8+ CTLs, while MHC class II molecules present exogenous peptides to CD4+ helper T cells, crucial for adaptive immune responses.[9] In contrast to T cells, NK cells do not express TCR signaling components like CD3, and express their own natural cytotoxicity receptors, like NKG2D, NKp46, NKp44 and NKp30.[10] In addition, NK cells can also express CD16, CD56 (also found on CD8+ T cells), and CD57, which are widely used in combinations to identify NK cells. CTLs and NK cells express Perforin and Granzyme B (GZMB), which work together to induce apoptosis in target cells by creating pores in the cell membrane and triggering intracellular caspase cascades, respectively. Deeper understanding of the interaction of cytotoxic immune cells within the tumor microenvironment (TME) will help to identify improved biomarkers and therapy selections for patients.[11]

In this analysis of a highly multiplexed 30-plex assay of a human CRC patient sample, we want to identify CTLs and NK cells based on the available assay panel markers CD8 for CTLs, CD56 as a surrogate marker for NK cells that was available in the assay panel (more specific NK cell markers such as CD16, NKp46 or NKG2D were not in this assay panel), and using GZMB as a marker for cytotoxicity on these cells. Here, we want to understand their relation to cytokeratin-expressing (CK+) epithelial cancer cells within the TME. To understand their spatial relationships within the TME, we analyze the general proximity of the CD8+GZMB+ and CD56+GZMB+ cell populations to CK+ cells and quantified the number of neighboring cells of these populations and their mean distances to each other. For this immune microenvironment characterization, we were using the Visiopharm Phenoplex workflow for multiplex and digital pathology image analysis.

Results

Visual QC and annotations

A visual inspection of this COMET 30-plex assay CRC patient sample provided by Lunaphore, a Bio-techne Company (Tolochenaz, Switzerland), shows that the CK+ areas (green) appeared to have two distinct TMEs: one with little to no Human Leukocyte Antigen - DR isotype (HLA-DR) expression (red) and the other with HLA-DR expression (Figure 1A and 1C). HLA-DR is a class II major histocompatibility complex (MHC) cell surface receptor mainly found on antigen presenting cells such as B cells, dendritic cells or macrophages and its main function is to present extracellularly derived peptide antigens to CD4+ T helper cells. HLA-DR is critical for the activation and orchestration of lymphocytes and the adaptive immune response. In CRC, expression of HLA-DR on cancer cells has potential implications in cancer immunology and therapy. The CK+HLA-DR+ double-expressing cells were clearly tumor epithelial cells as they did not express immune markers such as CD45, CD11b, or CD68 (Figure 1E and 1F).

Tissue Mapping

Tissue mapping (also known as tissue segmentation) was performed by training a deep-learning (DL) algorithm to recognize morphological features in the images. Training the algorithm was done through a paint-to-train process: the user hand-draws exemplary regions for each morphologic region they want to differentiate (tumor and stroma, for instance) and the deep-learning network creates an algorithm based on selected image channels (e.g., CK and DAPI) that will classify the images into those regions of interest (ROI), here named tumor and stroma.

For the analysis of the cytotoxic lymphocyte populations in this sample we planned to identify these cells in four distinct tissue compartments: the CK+ tumor epithelial area; the tumor associated stromal area; and two invasive-margin bands each extending 30 µm from the tumor-epithelial border into the stroma area. We added the invasive margin regions to better understand the epithelial-stroma interface and to highlight immune cell density, neighbor composition differences, and cellular distances to the tumor epithelial front in more detail. Furthermore, this can be used to map out where the interaction of cytotoxic lymphocytes with other immune populations occurs. Figures 1B and 1D show the mapping of this CRC patient sample into distinct regions, first using a DL algorithm to segment it into CK+ regions (considered tumor) and CK- regions (considered stroma). Then both tumor and stroma regions were subdivided manually into HLA-DR+/– status where: HLA-DR– tumor was masked in red; HLA-DR+ tumor masked by green; HLA-DR– stroma marked by blue; and HLA-DR+ stroma marked by yellow. Next, CK+ areas (tumor) were dilated into the stromal region in two 30 µm steps to generate Invasive Margin 1 (0-30 µm, IM1) and Invasive Margin 2 (30-60 µm, IM2) areas adjacent to each of the CK+ tumor masks. Here, TME is used to describe the tissue environment in and around the tumor, which is the sum of the ROIs for tumor, IM1 and IM2 combined. It excludes Stroma >60 µm from the epithelial tumor border. Tertiary Lymphoid Structures (TLS) in the tumor vicinity were identified by the specific patterns of CD3-expressing T cells around cores of CD20-expressing B cells and were isolated manually.

Figure 1

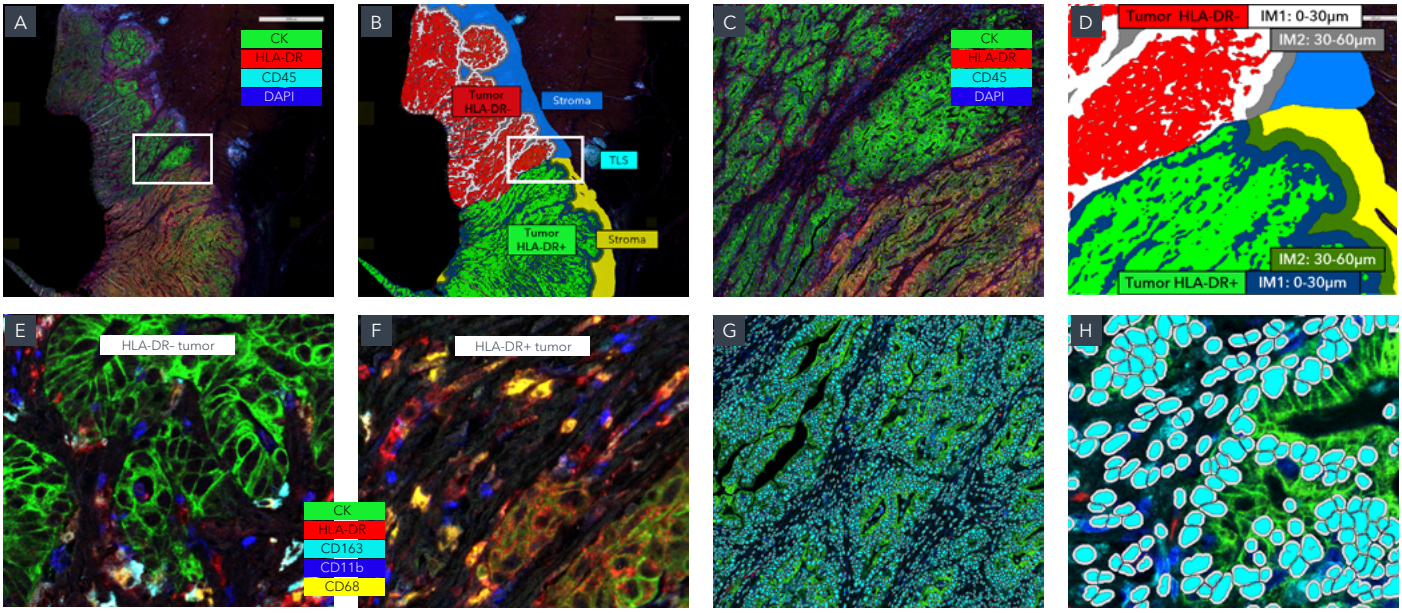

Figure 1: Tissue mapping and cell detection. A) overview of the CRC sample showing markers for CK (green), HLA-DR (red), and CD45 (cyan), and DAPI (blue). **B)** Tissue Mapping result of the CK segmentation APP (red and green ROIs are the tumor epithelial regions). Other regions are described in the legend. **C)** and **D)** Zoom into the region of adjacent CK+ and CK+HLA-DR+ tumor areas. Invasive margins (IM1 and IM2) of increasing 30 µm distance bands around the epithelial areas are shown in light grey and grey for regions adjacent to the CK+ red tumor area, and dark blue and dark green for regions adjacent to the CK+HLA-DR+ green tumor area. Stromal areas for the two tumor regions that are >60 µm away from the epithelial border are shown in blue and yellow. **E)** High magnification image of a CK+ HLA-DR– tumor nest, with clear HLA-DR expression (red) in stromal immune cells only. **F)** High magnification image of HLA-DR expression (red) on CK (green) and stromal cells. **G)** Blueprint APP DAPI cell segmentation results, detected nuclei are shown in cyan, and the expanded cytoplasm in grey. H) higher magnification of G.

The final tissue mapping shows the tumor ROI in red (HLA-DR–) and green (HLA-DR+), the stroma in blue (HLA-DR–) and yellow (HLA-DR+) plus all the invasive margin colors (white, grey, dark blue and forest green), and TLS shown in cyan. The invasive margin regions are: 0-30 µm from HLA-DR– (white), 30-60 µm from HLA-DR– (grey), 0-30 µm from HLA-DR+ (dark blue), and 30-60 µm from HLA-DR+ (forest green, Figures 1B and 1D).

This tissue mapping step was critical in allowing us to understand the entire context of the tissue while interrogating eight specific regions (IM1, IM2, Tumor, and Stroma, in the HLA-DR– and HLA-DR+ tumor ROIs) of this CRC patient tissue in more detail. Differences in phenotype and cell population distributions were measured not only across the tumor and normal tissue but also within HLA-DR+ and HLA-DR– microdomains of each of the tumor, associated stromal invasive margin bands, IM1 & IM2, and the rest of the stroma. Table 1 shows the final area tabulation for each of the eight regions that were isolated for analysis. You will notice that the analyzed area of each HLA-DR+ and HLA-DR– regions were similar, suggesting a similar number of total cells when comparing individual cellular densities between those two major regions of the image.

	ROI	Area (mm²)	Counts
HLA-DR-	Tumor	9.58	113,109
	IM1	5.27	55,720
	IM2	1.07	13,407
	Stroma	4.43	35,038
HLA-DR+	Tumor	9.66	115,014
	IM1	5.47	39,957
	IM2	0.59	4,845
	Stroma	1.99	10,402

Table 1: ROI area quantification in mm² and Cell Counts

Cell Phenotyping and Verification

After tissue mapping, the DAPI-based cell segmentation blueprint APP included with Phenoplex was used without modification to define all cellular objects (Figure 1G and H). The cellular boundaries defined by this APP for each cell including demarcation of the nucleus and outgrowth of a cytoplasmic compartment by postprocessing steps, allowing us to enrich for biomarker expression, if necessary, in one or both cellular compartments. All 30 protein biomarkers (see Table 2, excluding DAPI) of the assay were used in phenotyping the identified cellular objects, including: FOXP3, Ki67, LaminB1, CD11b, Caspase3, CD20, CD3, CD8, CD56, CD68, PD-L1, ASMA/αSMA, PD-1, CD45, LAG3, ZEB1, FAP, TAGLN, CD31, pH2AX, Vimentin, CK, GZMB, CD163, NaKATPase, HLA-DR, CD45-RA, MYL9, CD34, and Tryptase. Phenoplex's Guided Workflow was employed to set positivity conditions for each biomarker based on intensity and relevant cellular distribution. For example, αSMA positivity was gated on the intensity value of the total cell, i.e., both nuclear and cytoplasmic compartments, whereas CD3, CD56 and GZMB positivity were limited to the nuclear compartment to enrich for small lymphocytes that typically have low amounts of cytoplasm, resulting in reduced cellular signal crosstalk and improved phenotyping.

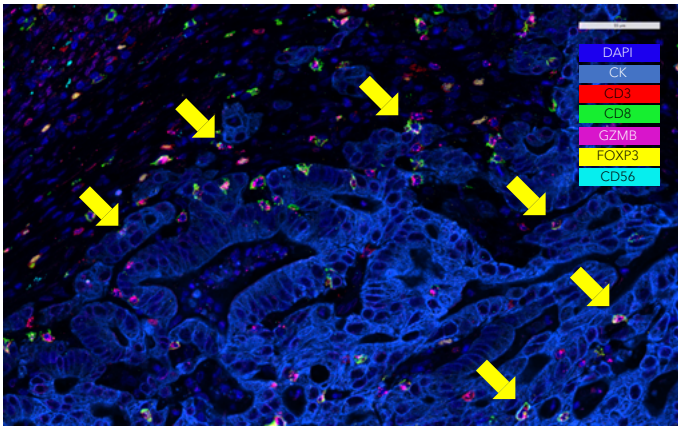

Figure 2: Representative field of view of the CRC TME showing the biomarkers DAPI (dark blue), CK (blue), CD3 (red), CD8 (green), GZMB (pink), FOXP3 (yellow), and CD56 (cyan). Note the distinct co-localization of GZMB within CD8- and CD56-expressing cells at the tumor-stroma interface. Yellow arrows pointing to exemplary cytotoxic cells with clear colocalization of CD56+GZMB+ and CD8+GZMB+.

We noticed that many cytotoxic immune cells were positioned within the TME of the CRC sample and that there was an obvious co-localization of GZMB (pink) in CD8+ T cells (green) and CD56+ NK cells (cyan) (Figure 2) within the cell objects. We wanted to understand the spatial distribution of CTLs and NK cells to each other and within the various microdomains of the tissue map that we had generated. The number of cells co-expressing every pair-wise biomarker combination was based on the positivity settings derived from Phenoplex's guided workflow. Phenoplex's Co-Occurrence Matrix (Figure 3A) allowed us to quickly review the number of co-positivity for two biomarkers in cells for each biomarker pair. This allowed us to interactively and quickly QC settings and adjust positivity gates as needed. Clicking on a box will highlight each of the cells in the original images that are positive for two biomarkers based on the threshold settings, allowing us to quickly see the distribution of each biomarker-pair phenotype. Based on the positivity settings, we found 22,387 CTLs (CD3+CD8+), of which 4,580 were activated CTLs, expressing GZMB (CD8+GZMB+), and 646 NK cells (CD56+GZMB+) (Figure 3A). By clicking on the box where CD3+ row intersects the CD8+ column in the Co-Occurrence Matrix, each of the 22,387 CD3+CD8+ double expressing cells are highlighted in the tissue (Fig.3B and E, yellow overlay dots). This reveals that most of these CD8+ immune cells were within the HLA-DR– (red ROI) area and to a lesser extent in the HLA-DR+ (green ROI) area (Figure 3B). This localization pattern appeared to also be true for CD8+GZMB+ CTLs and CD56+GZMB+ NK cells (Fig.3C and 3D), and other immune cell populations (data not shown here). The identified cells (yellow dots, Figure 3B - D) had an obvious co-localization pattern; at higher magnification the yellow dots indicate individual cells, co-expressing CD3+CD8+ (Figure 3E), CD8+GZMB+ (Figure 3F) and CD56+GZMB+. (Figure 3G).

Figure 3

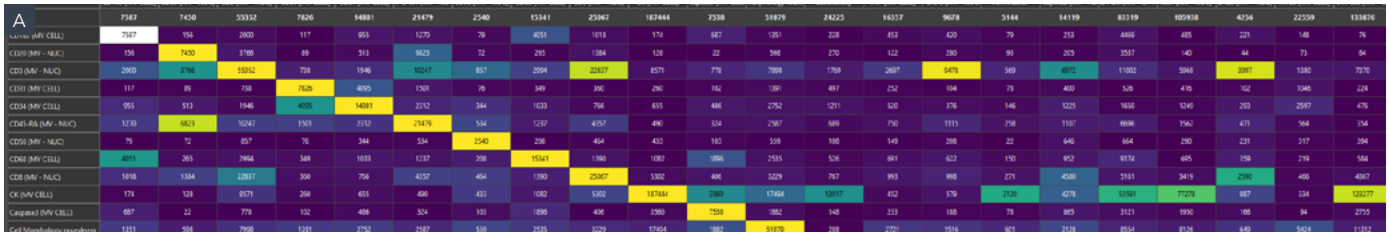

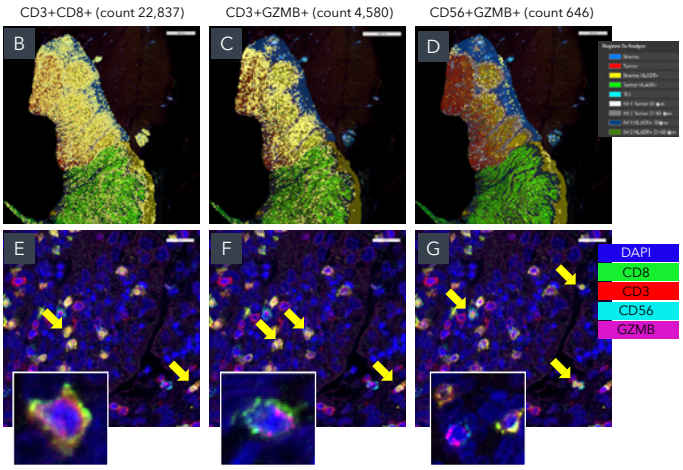

Figure 3: Interactive Co-Occurrence data review

A) Co-Occurrence Matrix display of 30 biomarkers (yellow = high cooccurrence, dark purple = low to no cooccurrence). **B** and **E)** CD3+CD8+ expressing cell distribution within the total tumor area, yellow dots show localization of double expressing cells. **C** and **F)** CD8+GZMB+ expressing cell distribution within the total tumor area, yellow dots show localization of double expressing cells. **D** and **G)** CD56+GZMB+ expressing cell distribution within the total tumor area, yellow dots show localization of double expressing cells. **E** – **G)** zoom in into high magnification, visualization of DAPI, CD8, CD3, CD56, GZMB. Inserts in E – G show exemplary high magnification cells for CD3+CD8+, CD8+GZMB+, and CD56+GZMB+.

It appeared that most of the CD8+GZMB+ CTLs were concentrated within the TME (Figure3C and 3F) whereas CD56+GZMB+ NK cells were mainly found at the interface of the IM1 and tumor epithelium in the HLA-DR– tumor and in the stroma within the HLA-DR+ tumor ROIs (Figure 3D and G). Each of these immune populations appeared to accumulate within the HLA-DR– portion of the tissue (see Figure 3B – D). The number of CD3+CD8+, CD8+GZMB+ and CD56+GZMB+ cells within HLA-DR– and HLA-DR+ tissue of four distinct areas were then counted in tumor, IM1, IM2, and stroma (Figure 4), which confirmed this observation. The HLA-DR+ tumor had less infiltration of CTL and NK cells compared to the HLA-DR– tumor. Both total and activated CTL counts were highest in the HLA-DR– tumor region; however, the activated (GZMB+) counts decreased by 90% in IM2 and stroma while the total CTL counts were reduced by only 20% in the stroma (Figure 4A and 4B). Cellular densities, which normalize the counts to the ROI area (cells/mm^2) showed that the highest densities of the CTLs was within IM2 (30-60 µm from the tumor epithelial border) of HLA-DR– region whereas the activated population had an even density throughout the TME (Figure 4D and 4E). In the HLA-DR+ TME, both total and activated CTLs had the highest density within IM1. On the other hand, CD56+GZMB+ NK cells were found to concentrate within IM2 and stroma, further away from the tumor, which was more pronounced in the HLA-DR+ area of the tissue (Figure 4F).

Figure 4

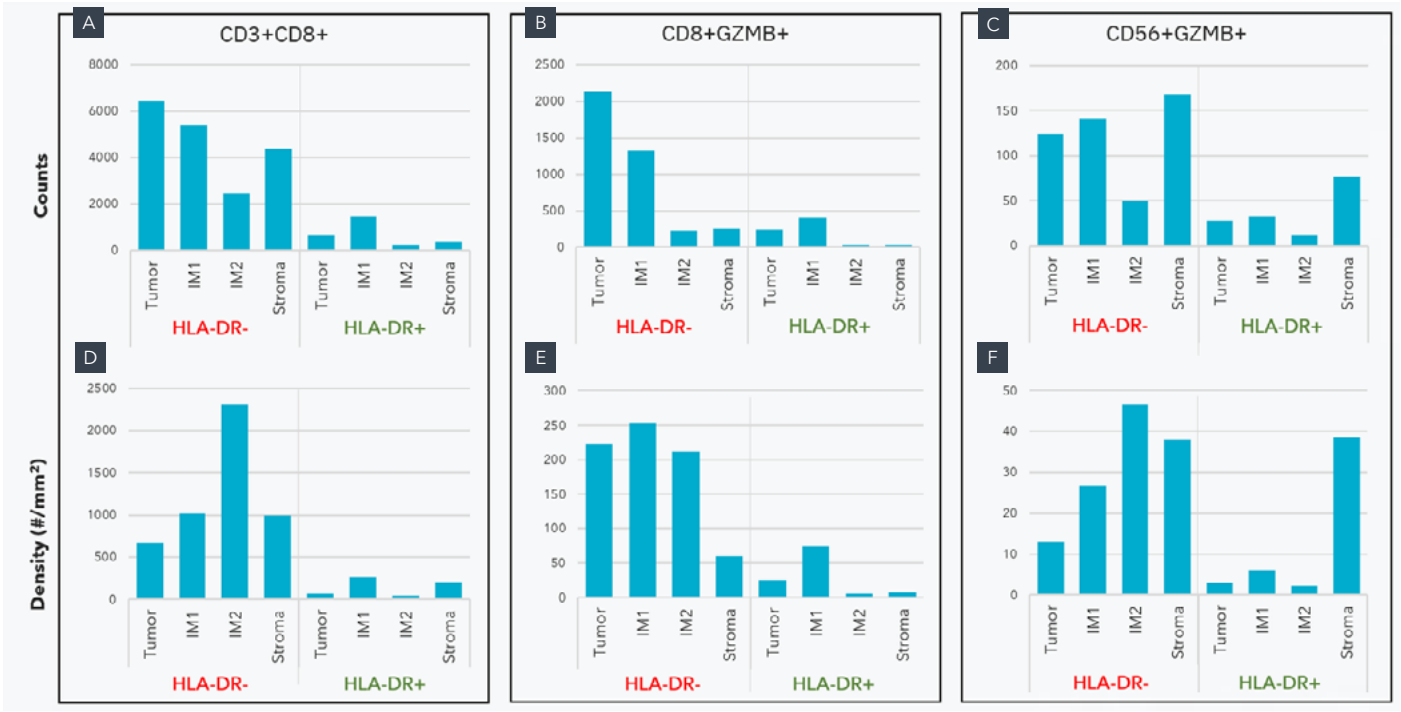

Figure 4: Total Cell Counts and Cell Densities. **A** and **D)** CD3+CD8+ expressing cells. **B** and **E)** CD8+GZMB+ expressing cells and **C** and **F)** CD56+GZMB+ expressing cells in the Tumor, Invasive Margin1 (IM1) and Invasive Margin 2 (IM2) and stromal area >60 µm from the tumor epithelial border (Stroma) inside the CK+ and CK+HLA-DR+ tumor environment.

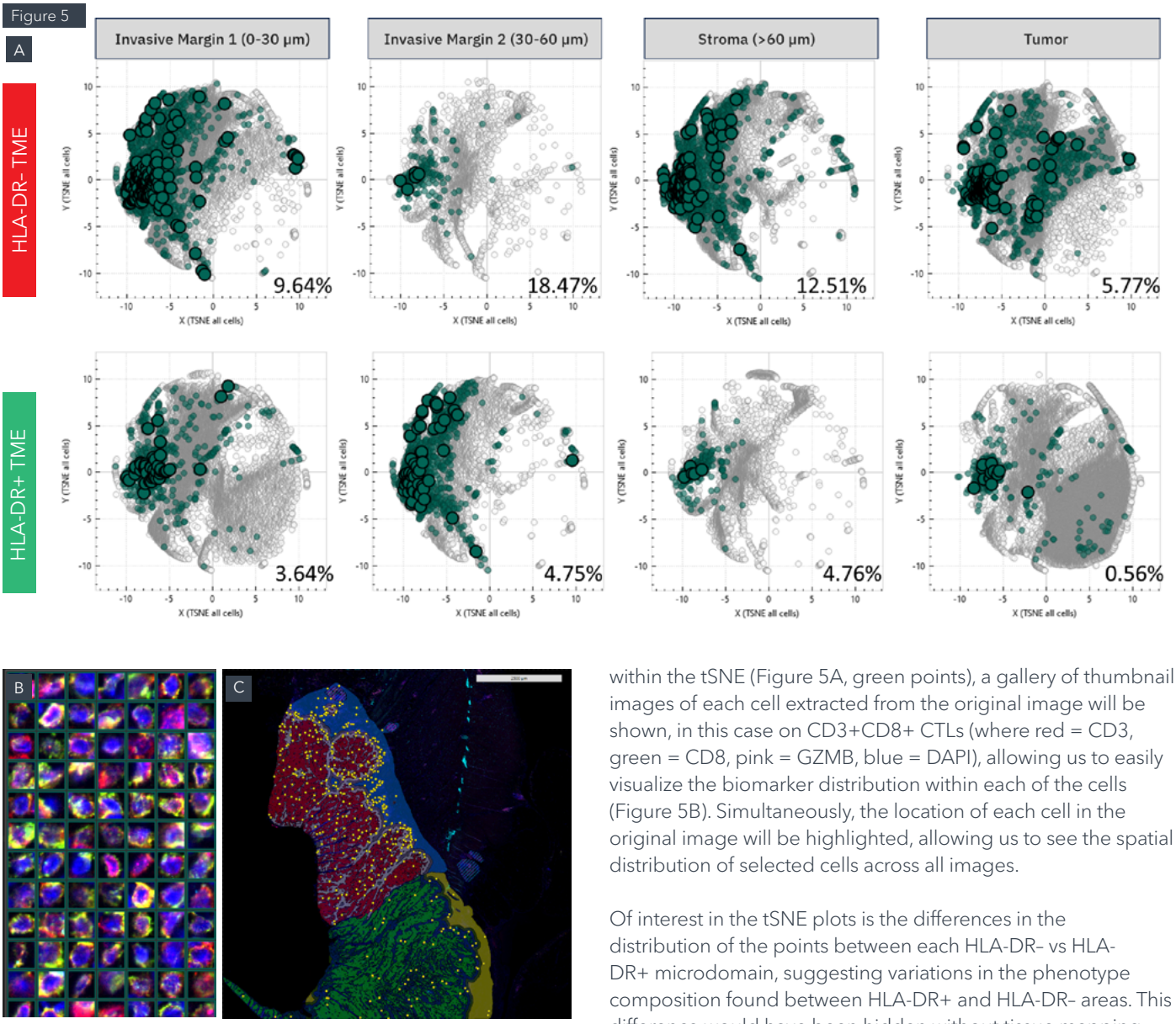

Figure 5: Data Exploration. Percent of cytotoxic T cells to total cell counts per tissue ROI. CD3+CD8+ cell objects are shown in green in the tSNE plots that are split by the ROIs for IM1, IM2, Tumor epithelium, and Stroma for the HLA-DR- and HLA-DR+ tumor parts. Randomly sampled cell objects for CD3+CD8+ population are shown as a cell gallery (middle) and are highlighted within the viewer as yellow overlays, to enable review of their location within the sample.

Data Exploration

The interactive multi-dimensional data reduction plotting feature included with Phenoplex allows the generation of a tSNE plot (where cells of similar biomarker expression patterns cluster closer to each other in a 2-dimensional graph) and then to split that plot into separate sub-tSNE plots, one for each variable used – in this case, each microdomain ROI. We found that the HLA-DR- areas had an overall higher percentage of the total cell population of cytotoxic lymphocytes within the tumor, IM1, IM2 and stroma compared to the same HLA-DR+ microdomains for these cells (Table 1). Visualizing cells positive for CD3+CD8+ within the tSNE subplots revealed that CTLs were 3-10x more concentrated in HLA-DR- vs HLA-DR+ microdomain (Figure 5A). When selecting cells (data points) within the tSNE (Figure 5A, green points), a gallery of thumbnail images of each cell extracted from the original image will be shown, in this case on CD3+CD8+ CTLs (where red = CD3, green = CD8, pink = GZMB, blue = DAPI), allowing us to easily visualize the biomarker distribution within each of the cells (Figure 5B). Simultaneously, the location of each cell in the original image will be highlighted, allowing us to see the spatial distribution of selected cells across all images.

Of interest in the tSNE plots is the differences in the distribution of the points between each HLA-DR- vs HLA-DR+ microdomain, suggesting variations in the phenotype composition found between HLA-DR+ and HLA-DR- areas. This difference would have been hidden without tissue mapping and splitting (faceting) the tSNE plot into subplots for individual microdomains but is readily observable with this analysis. Closer examination of the CD3+CD8 CTL populations showed that a higher percentage of these T cells were present in the HLA-DR- parts of the CRC tissue (Figure 5A green points) in line with the density measurements in Figure 4D. tSNE analysis allows us to also see which of the other 30 biomarkers may also be expressed in the CD3+CD8+ population and the differences between each microdomain. Additionally, we were also able to look at additional immune cell and non-immune cell phenotypes including T cells, macrophages, Cancer Associated Fibroblasts (CAF), and tumor epithelial cells.

For all CD3+ phenotypes we examined, T cell infiltration was elevated in the HLA-DR- areas of this CRC patient sample compared to HLA-DR+ areas (Figure 6A). We also found that CD56 was expressed on the CTLs, and densities for CD8+GZMB+ (HLA-DR-: 194.16 cells/mm^2 HLA-DR+: 39.20 cells/mm^2) and CD8+CD56+GZMB+ (HLA-DR-: 189.30 cells/mm^2 HLA-DR+: 37.39 cells/mm^2) were similar, so we continued with CD8+GZMB+. In the data exploration of the CD56+GZMB+ cells we did not find CD8 expressing cells,

Figure 6

therefore we continued with comparing CD8+GZMB+ as CTLs to CD56+GZMB+ as NK cells for this analysis. The reduced numbers in the HLA-DR+ areas of the tissue are not due to a lower total cell density (cells/mm^2 within the ROIs), as shown in Figure 5A. In fact, the density of CK+ tumor cells and CK+Ki67+ proliferating tumor cells are 1.54 – 2.27x higher in the HLA-DR+, unlike all other cell phenotypes tested (Figure 6B), even though the areas are nearly identical (Table 1). Tumor cells expressing PD-L1 were at a higher concentration in the HLA-DR– (77.32 cells/mm^2) area compared to HLA-DR+ (54.33 cells/mm^2). Overall, the counts and densities were low for both, suggesting that the immune infiltrate differences are not mainly mediated by PD-L1+ epithelial cells (Figure 6C).

Figure 6: Density Analysis. A) Quantification of T cell population densities in total HLA-DR– (red) and total HLA-DR+ tumor area (green) showed a higher density of all cell types in the HLA-DR– tumor microenvironment. **B)** the CK+HLA-DR+ tumor showed higher counts for CK+, CK+HLA-DR+, CK+Ki67+ compared to the HLA-DR– region. **C)** the CK+ tumor area (red) had higher densities for CK+PD-L1+ cells compared to the CK+HLA-DR+ area. **D)** CK+ tumor areas showed a higher density of ASMA+FAP+ CAFs, as well as a higher density of fibroblasts with an elongated morphology. **E)** + **F)** CK+ tumor ROIs showed a larger population and higher density in macrophages and M2-like PD-L1+ macrophages. **G** – **K)** detailed ROI analysis of densities for G) T cell populations of Tregs, **H)** exhausted LAG3+ T cell populations, **I)** macrophages, and **K)** FAP+ CAFs, within the epithelial tumor, invasive margin 1 (IM1) (0-30 µm), invasive Margin 2 (IM2) (30-60 µm), and stromal area (Stroma, >60 µm from tumor epithelial border).

Immunosuppressive CAF (FAP+ASMA+) and M2-like macrophages were concentrated in the HLA-DR– TME. In detail, FAP+ASMA+ CAFs showed a higher density within the HLA-DR– tumor (Figure 6D) (72.16 vs 40.44 cells/mm^2). Macrophages presented almost exclusively in the HLA-DR– area, while only a few M2-like macrophages (CD68+CD163+, 8.08 cells/mm^2) and almost no PD-L1+ macrophages were found in the HLA-DR+ area (0.85 cells/mm^2), see Figure 6E and 6F. A higher density of M1 macrophages (CD68+CD163–) were found in the HLA-DR+ (430.93 cells/mm^2) area compared to M2 macrophages (188.71 cells/mm^2). Interestingly, the density of the M2 macrophage population in the HLA-DR– was about 2/3 of the HLA-DR– population (M2 188.71 cells/mm^2 vs M1 430.93 cells/mm^2) in this CRC sample (Figure 6F), showing a higher M1 to M2 ratio in the HLA-DR– regions.

Detailed analysis of the TME microdomains are shown in Figure 6G-6K. Most of the T cells showed a density gradient from highest in IM2 and decreasing toward the tumor, suggesting that recruited T cells are being kept away from the tumor front, in the HLA-DR– portion of the cancer, and recruitment in the HLA-DR+ region of the cancer is inhibited (Figure 6G and 6H). Macrophages followed a similar pattern to the T cells but there was significant recruitment of M1 macrophages even in the HLA-DR+ IM1 and IM2 microdomains (Figure 6I). CAF densities were lowest in the HLA-DR+ regions, however, significant CAF recruitment was found in IM1 and IM2 in both HLA-DR areas, with HLA-DR– being slightly higher than the HLA-DR+ region (Figure 6K).

Spatial Neighborhood Analysis

After the spatial distribution of certain phenotypes has been established related to HLA-DR+/– microdomains, we measured the proximity profile of different phenotypic targets. For example, we found that in HLA-DR– areas, there was an average of 0.33 activated CTLs within a 15 µm radius of HLA-DR– tumor cells and an average of 1.00 when extending to a 30 µm radius (Figure 7A). On the other hand, these numbers drop to 0.05 and 0.16 respectively when looking at HLA-DR+ areas (Figure 7A). There were relatively few NK cells near tumor cells at a 30 µm radius under all conditions (< 0.06 cells). When looking at the reciprocal analysis, we found that each activated CTL was surrounded by about 0.40 tumor cells within 15 µm and 1.12 tumor cell within 30 µm in HLA-DR– and 0.60 and 1.74 respectively in HLA-DR+ tumor regions. NK cells in the HLA-DR– region had 0.46 tumor cells at 15 µm radius and 1.19 at 30 µm radius and in the HLA-DR+ region 0.89 at 15 µm and 2.20 in 30 µm distance on average. It was interesting that under the HLA-DR+ conditions, the target cells were closer to tumor cells

Figure 7

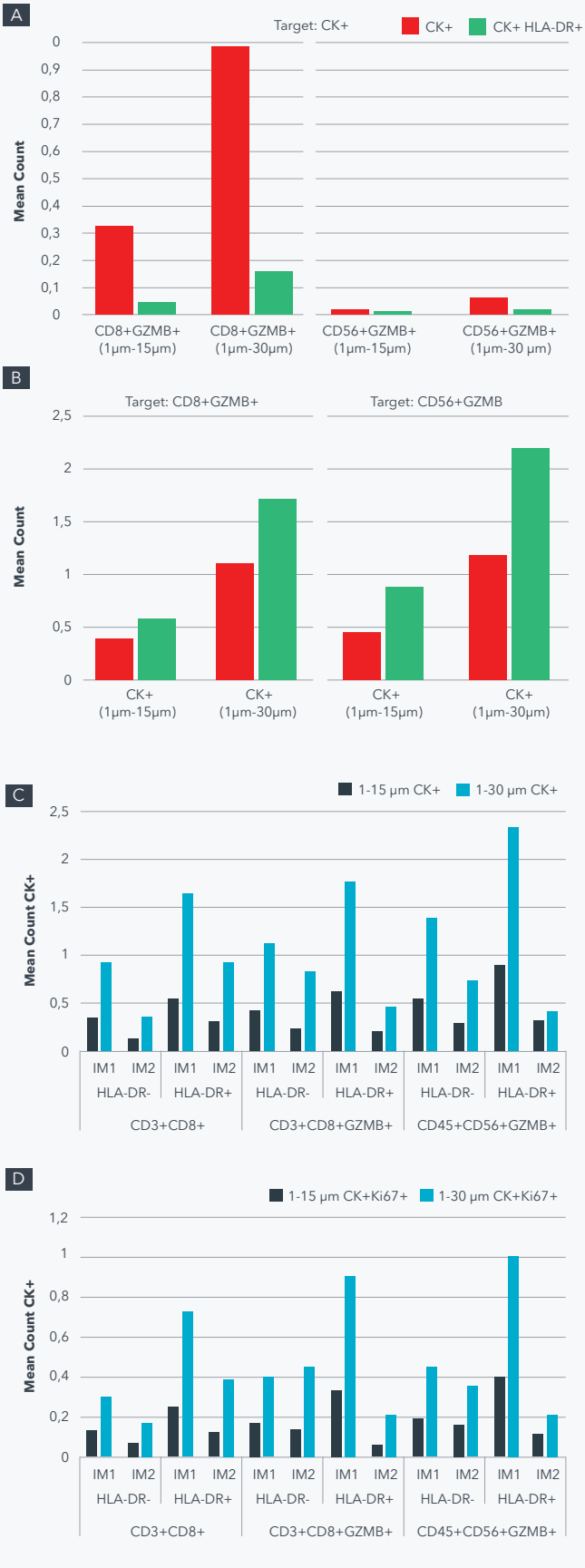

Figure 7: Proximity analysis

A) Average Neighbor counts of CD8+GZMB+ and CD56+GZMB+ within a 15µm and 30 µm radius around CK+ tumor epithelial cells,

B) Average Neighbor Counts of CK+ cells around cytotoxic CD8+GZMB+ and CD56+GZMB+ cells within 15µm and 30 µm; red bars are within the HLA-DR– tumor region, green bars are for HLA-DR+ tumor region, for both tumor types in the epithelial region ROI and the IM1 and IM2 ROIs were combined for analysis.

C) Detailed view of HLA-DR– cells within the IM1 and IM2 ROIs. Mean counts of CK+ cells around CD3+8+, CD8+GZMB+ and CD56+GZMB+ cells within 15 µm (blue bars) and 30 µm (orange bars). **D)** Analysis of CK+Ki67+ cells within the IM1 and IM2 ROIs. Mean counts of CK+Ki67+ cells around CD3+CD8+, CD8+GZMB+ and CD56+GZMB+ cells within 15 µm (blue bars) and 30 µm.

even though there was a much lower density (Figure 4). The propensity for a tumor cell to be in the vicinity of the immune cells in invasive margins 1 and 2 tended to be greater under the HLA-DR+ condition and favored the IM1 margin adjacent to the tumor (Figure 7C). We also found this trend to continue when looking at Ki67+ proliferating tumor cells (Figure 7D).

We were also interested in immunosuppressive Treg and PD-L1 expressing macrophage populations and wanted to know how many of these cells were on average within 15 µm of the cytotoxic lymphocyte populations. Figure 7E showed that IM2 had slightly higher average numbers of Treg CD3+FOXP3+ cells within the radius of 15 µm around the three cytotoxic lymphocyte populations in the HLA-DR– tumor. Similar observations were made for the M2-like PD-L1 expressing macrophages (CD163+PD-L1+ cells), which had a higher count around the cytotoxic lymphocyte populations in IM2 than IM1 in the HLA-DR– tumor. Thus, it is more likely to have these interactions further from the tumor.

Finally, we measured the average distance of each of the T cell and macrophage population phenotypes to the CK+ tumor cells. Overall, the mean distances were shorter in the HLA-DR– (Figure 8B, red) tumor compared to the results of the HLA-DR+ (Figure 8B, green). Comparing the mean distance from the cytotoxic lymphocyte populations CD3+CD8+, CD8+GZMB+, and CD56+GZMB within only the TME and excluding stroma, we found shorter mean distances from 6.6 to 13.5 µm to tumor cells and slightly further, 9.4 to 19 µm, to proliferating tumor cells (Figure 8C), with the shortest distance to a tumor cell being the CD8+GZMB+ population. Comparing the distances of the cytotoxic lymphocyte populations CD3+CD8+, CD8+GZMB+, and CD56+GZMB+ to other immune cells, we found that the mean distances for all four phenotypes were similar in each of the HLA-DR TMEs (figure 8D). However, in HLA-DR+ the phenotypes had a slightly higher distances to tumor cells compared to the HLA-DR– tumor. For example, CD3+CD8+ (14.7 µm in HLA-DR– and 39.1 µm in HLA-DR+) and CD8+GZMB+ cells (27.7 µm in HLA-DR– and 45.7 µm in HLA-DR+). Taken together, we found that the mean distance of the cytotoxic immune cell phenotypes to CK+ epithelial tumor cells and other immune cells was shorter in the HLA-DR– TME compared to the HLA-DR+ TME in this CRC sample.

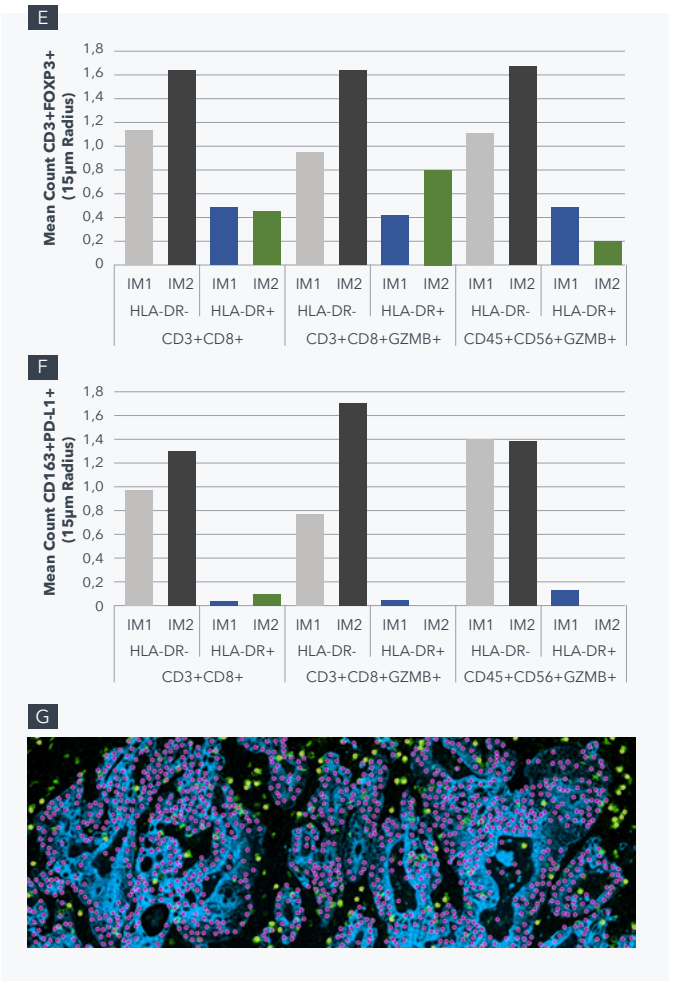

Figure 7 continued: Proximity analysis
E) Average Counts of CD3+FOXP3+ Treg cells around CD3+CD8+, CD8+GZMB+ and CD56+GZMB+ cells within 15 µm radius. **F)** Average Counts of CD163+PD-L1+ M2-like macrophages around CD3+CD8+, CD8+GZMB+ and CD56+GZMB+ cells within 15 µm radius. **G)** Tissue image from the HLA-DR- part with CD3+CD8 targets (yellow) and CK+ neighbors (magenta) within a 30µm radius.

Figure 8: Nearest neighbor distance analysis
A) overview of the tissue compartments, HLA-DR– tumor region (red), HLA-DR+ tumor region (green). **B)** Average distance of immune cells to CK+ tumor epithelial CRC cells in the HLA-DR– (red) and HLA-DR+ (green) tumor regions. **C)** Mean distance of cytotoxic lymphocyte populations to a CK+ or CK+Ki67+ expressing cell.

Figure 8

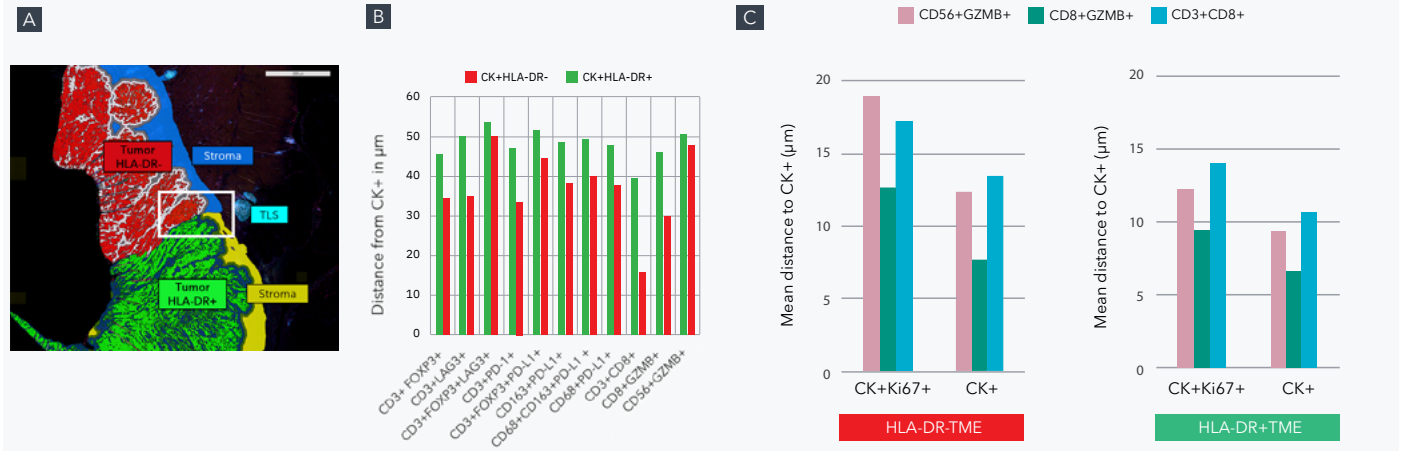

Figure 8 continued: Nearest neighbor distance analysis of the sample.
D) Mean distance of cytotoxic lymphocyte populations to other immune cell phenotypes within the HLA-DR– and HLA-DR+ tumor part.

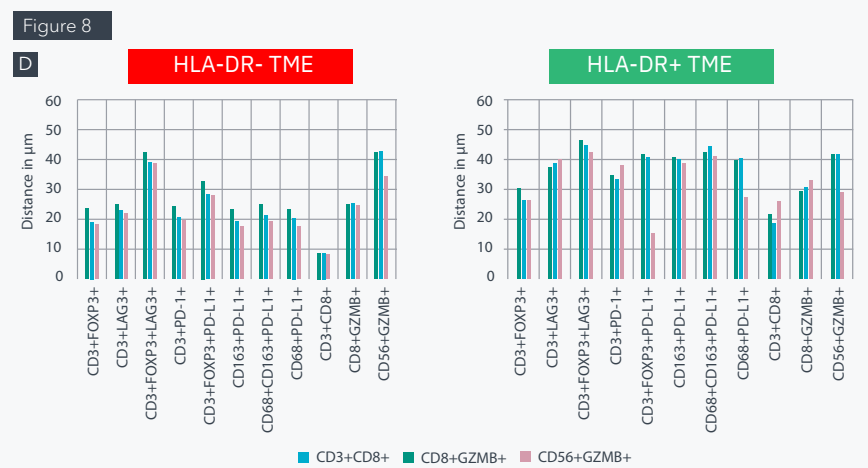

Summary

In summary, we have shown that this CRC patient sample that was stained with a 30-plex assay had two very distinct TME microdomains that correlated with the expression of HLA-DR on tumor cells. While the HLA-DR– tumor region showed higher invasion with CTLs within the stromal areas and the tumor epithelial area, this was strongly reduced in the equivalent HLA-DR+ areas within this sample (Figure 9). This result was validated using spatial analysis for proximity and distance analysis. Additionally, the HLA-DR– tumor-associated stroma showed higher overall densities for immunosuppressive cells, such as PD-L1 expressing macrophages and T cells, FOXP3+ T reg cells, and FAP+ CAF.

In general, based on the immune cell density results for this CRC sample, one could sub-categorize the HLA-DR– tumor part as immune inflamed and the HLA-DR+ tumor part as immune excluded, as most immune cells are found within the Invasive Margin 1 and 2 in the immune excluded region.[12] Without the detailed tissue segmentation, it would not have been possible to understand the differences between the HLA-DR– and the HLA-DR+ TME (Figure 9).

Given that this is based on only one sample, we could not identify a sound hypothesis for the differences in immune cell infiltration or proliferation capacity of the HLA-DR– vs HLA-DR+ tumor parts. Studies have shown that a strong expression of HLA-DR on cancer cells showed better prognosis of CRC patients.[13,14] While it has been reported that HLA expression is correlated with intra-tumoral lymphocytic infiltration, this CRC case shows the opposite relationship with respect to immune cells.[13] In another study by Matsushita et al.[14], strong HLA-DR-positive expression on cancer cells was significantly correlated to better prognosis for CRC patients. There they found that high IFN-gamma mRNA expression in situ was correlated significantly with reduced activation of c-myc mRNA expression in the analyzed samples.[14] A larger cohort study would be needed to understand how these immune infiltration differences differ between patients.

A deep-dive analysis like this using multiplex technologies can improve our understanding of tumor and disease biology and has the potential to inform treatment strategies for precision medicine in the treatment of patients. While anti-PD-(L)1 immune checkpoint inhibitors might provide a benefit for the HLA-DR– tumor portion, they might not show effects on the HLA-DR+ tumor clone. A larger cohort of CRC samples stained with this assay panel as well as additional markers for checkpoints like CTLA-4, TIM-3, or Adenosine pathway (CD73, CD39) expression in T cells and stroma, c-myc or dMMR related protein expression (MLH1, MSH2, MSH6, PMS2)[15] could further help to understand the mechanism behind immune cell exclusion and infiltration in CRC samples such as this one. Furthermore, tumor mutational burden analysis, metabolite data through MALDI-TOF, or transcriptomic analysis on the same or consecutive sections, would be approaches to enhance and complement the COMET data set in further experiments.

All analysis presented here was performed in Phenoplex or on data generated by Phenoplex. The interactive capabilities of Phenoplex allowed us to quickly identify pertinent cell types, find them within a tissue map, define their spatial relationships in the tissue, and analyze their neighbors. Through this process, we continued to ask more and more hypothesis-driven multiplex questions and were quickly able to find the answers, enabling better planning of the next round of experiments. Phenoplex is flexible, allowing for a quick analysis or opening the possibility for a deep-dive into regional tissue sample analysis, providing all the necessary A.I.-driven tools to support you, wherever your research takes you.

Figure 9

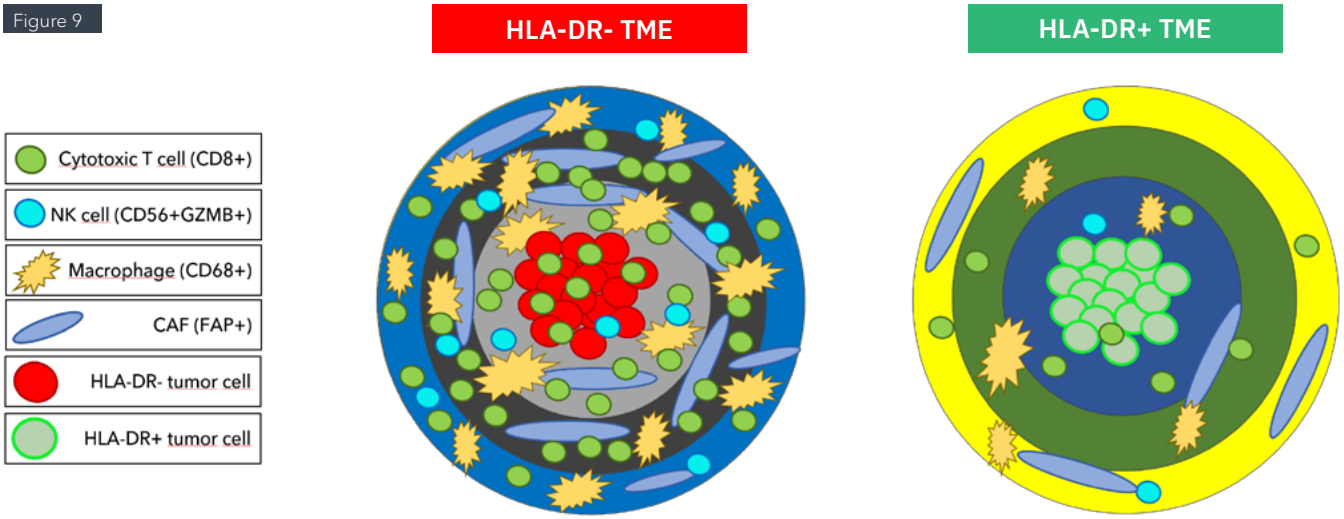

		HLA-DR- Cell Densities (cells/mm²)				HLA-DR+ Cell Densities (cells/mm²)			
		Tumor	IM1	IM2	Stroma	Tumor2	IM1	IM2	Stroma
T cells	CD3+CD8+	669.0	1019.1	2305.8	989.7	66.9	266.2	43.6	196.6
	CD8+GZMB+	222.6	252.4	211.4	59.2	25.1	74.3	5.7	8.0
	CD3+CD8+GZMB+	219.0	248.0	201.1	52.4	24.0	72.4	4.4	5.5
	CD3+PD-1	123.6	422.0	849.3	356.2	20.1	92.0	8.9	28.7
	CD8+PD-1+	54.2	159.6	380.9	131.9	3.3	19.6	2.8	4.0
	CD3+FOXP3+	24.5	123.7	254.2	94.6	6.4	53.6	9.1	15.1
	CD3+FOXP3+PD-L1	18.1	195.6	363.2	42.9	2.0	9.9	0.6	0.5
	CD3+LAG3+	105.9	288.2	434.9	124.0	9.7	46.5	4.2	15.1
	CD3+LAG3+PD-L1+	23.9	118.6	210.5	26.9	1.4	3.8	0.6	2.0
NK cells	CD56+GZMB+	12.9	26.8	46.6	37.9	2.9	6.0	2.3	38.7
Macrophages	CD68+CD163-	134.4	750.8	1230.2	498.0	33.0	285.8	687.2	99.5
	CD68+CD163+	36.9	223.5	539.2	390.7	1.7	16.6	27.0	10.1
	CD163+PD-L1+	244.0	822.0	410.0	459.0	4.0	10.0	1.0	0.0
	CD68+PD-L1+	374.0	1958.0	824.0	653.0	16.0	45.0	10.0	7.0
	CD68+CD163+PD-L1+	130.0	572.0	281.0	336.0	1.0	8.0	1.0	0.0
CAF	FAP+MYL9+	53.2	526.2	399.5	62.6	20.4	208.0	10.1	1.0
	ASMA+FAP+ elongated	6.4	33.8	6.5	3.2	1.4	13.2	1.7	14.1
	FAP+ elongated	24.9	136.0	75.4	24.6	11.4	59.1	10.1	57.3
	ASMA+FAP+	22.0	186.9	145.3	26.4	5.2	83.8	23.6	97.5

Figure 9: Summary Figure, showing the differences between the HLA-DR- and HLA-DR+ TME compositions of cytotoxic T cells, NK cells, macrophages and CAFs for this CRC sample. Tumor cells are shown at the center of the model figures (red, and grey with green border cells); invasive margins IM1 (grey and dark blue), IM2 (dark grey and forest green), and stroma (blue and yellow) are shown as concentric circles. Stromal populations are shown as representative densities comparing the two TME types (HLA-DR- and HLA-DR+) and represent densities in a qualitative manner to illustrate the differences between the "Immune Invasive" and "Immune Excluded" TMEs. Data table shows densities of analyzed phenotypes within the ROIs, tumor, IM1, IM2, and stroma, in the HLA-DR- and HLA-DR+ TME.

Position	Marker	Cell type
1	FOXP3	Regulatory T cell
2	Ki-67	Proliferating cell
3	LaminB1	Nuclear envelope
4	CD11b	Monocyte/macrophage
5	Caspase 3	Apoptotic cell pathway activator
6	CD20	B cell
7	CD3	T cell
8	CD8	Cytotoxic T cell
9	CD56	NK cell, peripheral nerve
10	CD68	Monocyte/macrophage
11	PD-L1	Immunosuppressive cell
12	αSMA/ASMA	Fibroblast, smooth muscle
13	PD-1	Active/exhausted T cell
14	CD45	Leukocyte
15	LAG3	Activated T cell
16	ZEB1	Endothelial/ mesenchymal cell
17	FAP	Activated Fibroblast
18	TAGLN	Fibroblast, smooth muscle cells
19	CD31	Endothelial cell
20	pH2AX	DNA-damaged cell
21	Vimentin	Mesenchymal cell
22	CK	Epithelial cell
23	Granzyme B	Serine protease in granules of Cytotoxic T and NK cells
24	CD163	Monocyte/macrophage/DC
25	NaKATPase	All cell type
26	HLA-DR	B cell, monocyte
27	CD45-RA	Naïve T cell
28	MYL9	Muscle cells, Fibroblast
29	CD34	Endothelial cell
30	Tryptase	Mast cell

Table 2: 30-plex assay biomarker overview

Literature

1. Garborg, K., Holme, Ø., Løberg, M., Kalager, M., Adami, H.O., and Bretthauer, M. (2013). Current status of screening for colorectal cancer. Annals of Oncology 24, 1963–1972.
→

2. Chan, T.A., Yarchoan, M., Jaffee, E., Swanton, C., Quezada, S.A., Stenzinger, A., and Peters, S. (2019). Development of tumor mutation burden as an immunotherapy biomarker: utility for the oncology clinic. Annals of Oncology 30, 44–56.
→

3. Samstein, R.M., Lee, C.-H., Shoushtari, A.N., Hellmann, M.D., Shen, R., Janjigian, Y.Y., Barron, D.A., Zehir, A., Jordan, E.J., Omuro, A., et al. (2019). Tumor mutational load predicts survival after immunotherapy across multiple cancer types. Nat Genet 51, 202–206.
→

4. Masugi, Y., Abe, T., Ueno, A., Fujii-Nishimura, Y., Ojima, H., Endo, Y., Fujita, Y., Kitago, M., Shinoda, M., Kitagawa, Y., et al. (2019). Characterization of spatial distribution of tumor-infiltrating CD8+ T cells refines their prognostic utility for pancreatic cancer survival. Modern Pathology 32, 1495–1507.
→

5. Galon, J., Costes, A., Sanchez-Cabo, F., Kirilovsky, A., Mlecnik, B., Lagorce-Pagès, C., Tosolini, M., Camus, M., Berger, A., Wind, P., et al. (2006). Type, Density, and Location of Immune Cells Within Human Colorectal Tumors Predict Clinical Outcome. Science (1979) 313, 1960–1964.
→

6. Tada, K., Kitano, S., Shoji, H., Nishimura, T., Shimada, Y., Nagashima, K., Aoki, K., Hiraoka, N., Honma, Y., Iwasa, S., et al. (2016). Pretreatment Immune Status Correlates with Progression-Free Survival in Chemotherapy-Treated Metastatic Colorectal Cancer Patients. Cancer Immunol Res 4, 592–599.
→

7. Vesely, M.D., Kershaw, M.H., Schreiber, R.D., and Smyth, M.J. (2011). Natural Innate and Adaptive Immunity to Cancer. Annu Rev Immunol 29, 235–271.
→

8. Vojdani, A., Koksoy, S., Vojdani, E., Engelman, M., Benzvi, C., and Lerner, A. (2024). Natural Killer Cells and Cytotoxic T Cells: Complementary Partners against Microorganisms and Cancer. Microorganisms 12, 230.
→

9. Klein, L., Kyewski, B., Allen, P.M., and Hogquist, K.A. (2014). Positive and negative selection of the T cell repertoire: what thymocytes see (and don't see). Nat Rev Immunol 14, 377–391.
→

10. Barrow, A.D., Martin, C.J., and Colonna, M. (2019). The Natural Cytotoxicity Receptors in Health and Disease. Front Immunol 10.
→

11. Angelova, M., Charoentong, P., Hackl, H., Fischer, M.L., Snajder, R., Krogsdam, A.M., Waldner, M.J., Bindea, G., Mlecnik, B., Galon, J., et al. (2015). Characterization of the immunophenotypes and antigenomes of colorectal cancers reveals distinct tumor escape mechanisms and novel targets for immunotherapy. Genome Biol 16, 64.
→

12. Tiwari, A., Oravecz, T., Dillon, L.A., Italiano, A., Audoly, L., Fridman, W.H., and Clifton, G.T. (2023). Towards a consensus definition of immune exclusion in cancer. Front Immunol 14.
→

13. Sconocchia, G., Eppenberger-Castori, S., Zlobec, I., Karamitopoulou, E., Arriga, R., Coppola, A., Caratelli, S., Cesare Spagnoli, G., Lauro, D., Lugli, A., et al. (2014). HLA Class II Antigen Expression in Colorectal Carcinoma Tumors as a Favorable Prognostic Marker. Neoplasia 16, 31-W15.
→

14. Matsushita, K., Takenouchi, T., Shimada, H., Tomonaga, T., Hayashi, H., Shioya, A., Komatsu, A., Matsubara, H., and Ochiai, T. (2006). Strong HLA-DR antigen expression on cancer cells relates to better prognosis of colorectal cancer patients: Possible involvement of c-myc suppression by interferon-in situ. Cancer Sci 97, 57–63.
→

15. Sacdalan, D.L., Garcia, R.L., Diwa, M.H., and Sacdalan, D.B. (2021). Clinicopathologic Factors Associated with Mismatch Repair Status Among Filipino Patients with Young-Onset Colorectal Cancer. Cancer Manag Res Volume 13, 2105–2115.
→